*Int. J. Solids Structures* Vol. 23, No. 12, pp. 1581–1600, 1987
Printed in Great Britain.

0020-7683/87 $3.00+.00


# THE DYNAMIC BEHAVIOUR OF SHARP V-NOTCHES UNDER IMPACT LOADING

P. S. THEOCARIS and G. A. PAPADOPOULOS
Department of Engineering Sciences, The National Technical University of Athens, P.O. Box 77230, Palaion Phaleron (17510), Athens, Greece

(*Received* 4 *November* 1986)

**Abstract**—The dynamic behaviour of sharp V-notches which are either symmetric or oblique to the longitudinal boundary of a homogeneous elastic and isotropic strip subjected to an impact plane pulse was studied by the method of caustics. The stress pulse impinging on the flanks of the notch reflects and diffracts in different ways depending on the geometry of the notch relative to the coming pulse. For compressive stress pulses a stress concentration at the bottom of the notch does not create a crack propagation phenomenon, whereas for tensile pulses there is a possibility for an incubation, nucleation and eventual propagation of a crack. A complete experimental study of the incubation nucleation and propagation of cracks from the bottoms of notches in thin strips under tensile stress pulses was undertaken, whereas for compressive stress pulses the stress concentration at the bottom of the notch was evaluated. Interesting results were disclosed concerning the reinforcement of pulses by reflection and caging in, the evolution of stress concentration at the notch and the mode of crack propagation inside the plate. Dynamic stress intensity factors were evaluated all over the paths of crack propagation indicating a close intimacy between crack velocity and values of SIFs.

## 1. INTRODUCTION

Stress wave propagations in infinite plates due to various types of stress pulses were extensively studied. Mathematical analyses of these phenomena have been presented by Kolsky[1], Sherwood[2], Cagniard[3], and Ewing *et al.*[4]. On the other hand, phenomena of fracture by stress waves were presented by Miklowitz[5], Thiruvenkatachar[6], Eichelberger[7], Broberg[8], Rinehart[9] and others. A mathematical analysis of the crack propagation in an elastic solid by an incident stress pulse was given by Freund[10, 11]. These references, however, constitute only a small part from a long list of papers concerned with dynamic fracture by impact.

Dynamic crack propagation studies under impact loading were advanced analytically and experimentally to yield information concerning crack initiation, acceleration, bifurcation and arrest. In this context the early and important work by Schardin should be mentioned[12]. Moreover, Kalthoff and Shockey[13] investigated the crack-propagation behaviour in a circular plate made of PC and subjected to impact, while Kobayashi *et al.*[14] made a similar study in a plate made of another birefringent polymer. On the other hand a mathematical analysis of crack growth under the influence of a stress wave was presented by Homma *et al.*[15].

Experimental studies of the dynamic behaviour of artificially cracked plexiglas strips under plane stress pulses created by projectiles shot from an air-gun have been presented in Refs [16, 17] by applying the method of caustics. The case of oblique edge cracks in long strips under impact was studied in Refs [18, 19]. In all these studies it was perceived that the initial edge crack is propagated by steps under the action only of the tensile stress pulses while the compressive pulses did not create any crack propagation. In all these studies it has been shown that any fluctuations of crack velocities and variations of the values of SIFs may be accurately detected by the positions, shapes, and sizes of the caustics.

The methodology developed in the previous studies was extensively used in a large number of papers by the senior author and his co-workers to study the complicated phenomena of crack propagation in composite plates representing either fibre-reinforced or particulate composites. For a general reference of these papers the reader is referred to the review chapter in Ref. [20].

In this paper the important problem of the dynamic behaviour of an edge V-notched

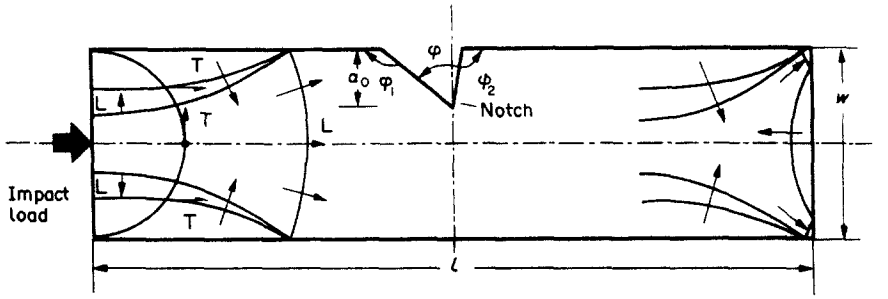


Fig. 1. Stress waves in plates indicating their splitting into dilatational or longitudinal (L), and distortional or transverse or shear (T) components.

thin strip submitted to a plane impact pulse was studied by using the method of caustics and pseudocaustics, especially when the notch is unsymmetrically placed relative to the transverse axis of the strip. Phenomena of reflection and diffraction of stress waves generated by the propagating stress pulse were studied in detail and their influence was taken into account up to their attenuation. The incubation, nucleation and propagation of cracks from the bottoms of the notches were studied in detail. The instantaneous values of the components of SIFs and the crack velocity were recorded and important results were derived from their study.

## 2. REFLECTIONS OF ELASTIC WAVES FROM THE NOTCH FLANKS

Figure 1 presents the modes of propagation and reflection of longitudinal (L) and transverse (T) stress waves. It is well known[1] that when a wave is impinging on the notch flanks, reflections take place along the free boundaries of its flanks. The amplitudes of the reflected L- or T-waves are inferior than the respective amplitudes of the incident waves for angles of incidence between zero and $\pi/2$. For angles of incidence equal to zero the amplitude of the reflected wave equals the amplitude of the impinging wave, but reverses its sign. Moreover, for normal incidence, the reflected wave is always of the same type as the incident wave, whereas for angles of incidence between zero and $\pi/2$ two types (dilatational (L) and distortional (T)) of waves are created. If the normally incident stress wave is compressive, the reflected wave is a tensile wave with amplitude equal to the amplitude of the impinging wave.

Figure 2 presents the reflections of a dilatational wave on the flanks of the notch. In Fig. 2(a) the V-notch of angle $\varphi$ has its flanks subtending angles $\varphi_1$ and $\varphi_2$ with the

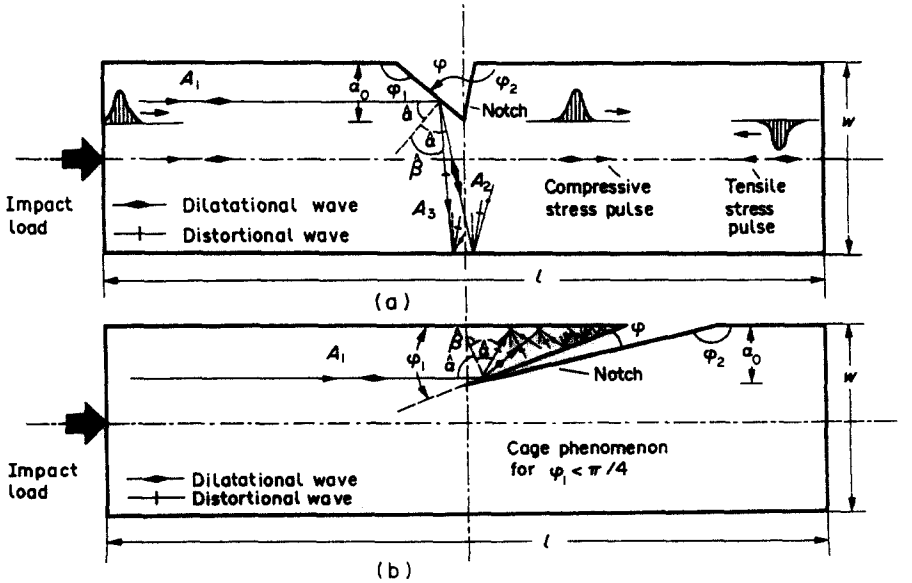


Fig. 2. Reflection of dilatation waves on the notch flanks of specimens.

longitudinal boundary of the strip for which it is valid that $\varphi_1 > \varphi_2 > \pi/2$. The angle of incidence of the dilatational wave is $\alpha = (\varphi_1 - \pi/2)$. Two component waves are reflected from the flank of the notch, a dilatational wave at an angle $\alpha$, and a distortional wave at an angle $\beta < \alpha$. The amplitudes of the reflected waves $A_2$ and $A_3$ are smaller than the amplitude $A_1$ of the incident dilatational wave. Subsequently, the two reflected waves along the closer notch flank impinge on the opposite longitudinal free boundary of the strip and secondary reflections take place.

In Fig. 2(b) the V-notch of an angle $\varphi$ has its flanks subtending angles $\varphi_1$ and $\varphi_2$ with the longitudinal boundary of the strip equal to $\varphi_1 < \pi/4$ and $\varphi_2 > \pi/2$. The angle of incidence of the dilatational wave is $\alpha = (\pi/2 - \varphi_1)$. As in the case of Fig. 2(a) two component waves are reflected from the closest flank to the arriving pulse, a dilatational wave at an angle $\alpha$ and a distortional wave at an angle $\beta$. The amplitudes of the reflected waves $A_2$ and $A_3$ are again smaller than the amplitude $A_1$ of the incident wave. Subsequently, the two reflected waves impinge on the closer longitudinal free boundary of the strip and four component waves are reflected from it, each of them impinging again on the same flank of the notch. The new four component waves give eight new component waves from the reflections on the flank of the notch and so on. However, the amplitudes of the reflected component waves tend to zero, but all reflected waves remain inside the region included between the longitudinal boundary and the flank of the notch, which is of an angle $\varphi_1$.

Thus, for angles $\varphi_1 < \pi/4$ a *cage-in phenomenon* of the waves is observed, while for angles $\varphi_1 \geqslant \pi/4$ such a cage-in phenomenon disappears[19].

## 3. DIFFRACTION OF ELASTIC WAVES AT NOTCH FLANKS

When a plane longitudinal stress pulse impinges on one flank of a notch in a plane-stress field, it is partially reflected and partially diffracted around the bottom of the notch. Then, a transient stress field is developed around the bottom, because of the refraction of the stress field. A mathematical analysis of the problem of diffraction of the flat front of a stress pulse in the region surrounding the crack tip was given in Refs [10, 11]. According to this theory of diffraction, if a plane longitudinal compressive or tensile pulse impinges along the bottom of the notch, it diffracts about this bottom and creates a compressive or tensile stress field, respectively, in the neighbourhood of the apex of the notch.

The mechanism of creation of such fields is indicated in Figs 3–6 for various types of sharp V-notches. The compressive or the tensile stress field introduces normal $\sigma_{\varphi_1}$- and $\sigma_{\varphi_2}$-stresses along the notch flanks and shear $\tau_{\varphi_1}$- and $\tau_{\varphi_2}$-stresses, which are dependent on angles $\varphi_1$ and $\varphi_2$, respectively, whereas the singularity of the stress field at the apex of the notch is dependent on the angle of the notch $\varphi$[21, 22]. Thus, the notch is under the influence of simple symmetric $(\sigma_{\varphi_1}, \sigma_{\varphi_2})$ and antisymmetric $(\tau_{\varphi_1}, \tau_{\varphi_2})$ states of stress.

The tensile stress field, which radiates around the apex, because of the diffraction of the tensile stress pulse at this apex and in front of it, originates the incubation and nucleation of a crack and may initiate its eventual propagation after some time lapse. The delay time for the incubation and initiation of propagation of a crack is due to the fact that enough energy must be stored at the bottom of the notch, so that the value of the respective stress intensity factor $K_1$ reaches its critical $K_{1C}$ value for propagation of the crack.

The values of $\sigma_{\varphi_1}$-, $\sigma_{\varphi_2}$- and $\tau_{\varphi_1}$-, $\tau_{\varphi_2}$-components of stress depend on the values of the respective velocities of the longitudinal and shear waves, the amplitude of the pulse and the angles $\varphi_1$ and $\varphi_2$. The diffracted pulse travels along the part of the strip behind the notch, it impinges normally along its transverse boundary, and then reflects backwards as a pulse of opposite sign (Fig. 2), since the transverse boundary of the strip is a free boundary. The reflected pulse impinges again on the notch flanks and creates similar phenomena, but of opposite sign.

Figure 3 presents the diffraction phenomenon of the stress pulse at a notch symmetrically placed to the direction of pulse propagation for (a) a compressive and (b) a tensile stress pulse. The compressive stress field introduces a normal $\sigma_{\varphi_1}$-stress along the notch flanks (Fig. 3(a) B) and a shear $\tau_{\varphi_1}$-stress (Fig. 3(a) C). The tensile stress field introduces a normal $\sigma_{\varphi_1}$-stress along the notch flanks (Fig. 3(b) B) and a shear $\tau_{\varphi_1}$-stress

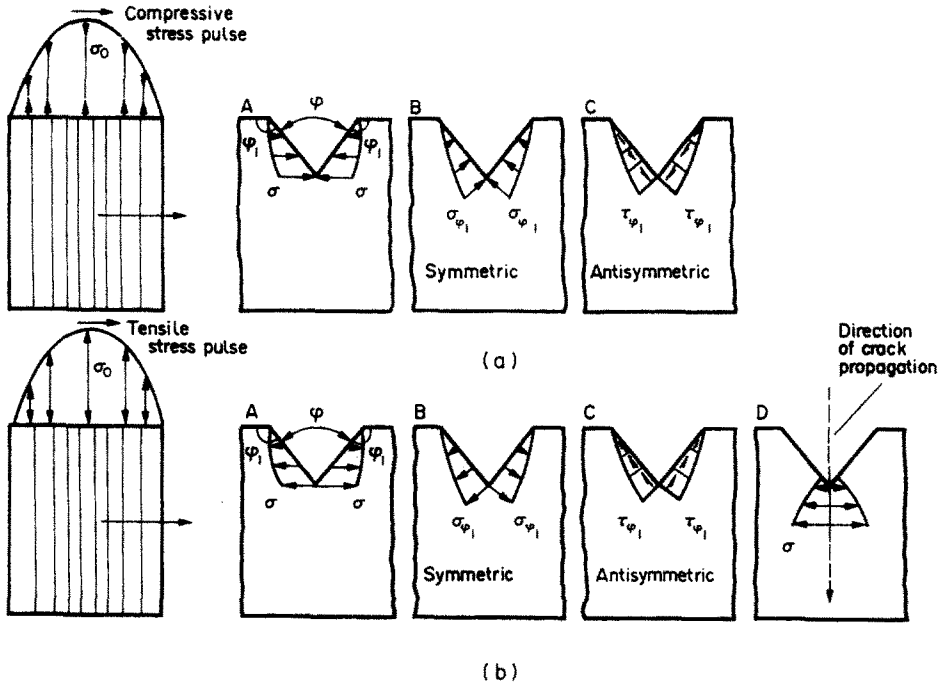


Fig. 3. Diffraction of the stress pulses at symmetric V-notches of an initial depth $a_0$: (a) compressive stress pulse; (b) tensile stress pulse, $\varphi_1 > 90°$.

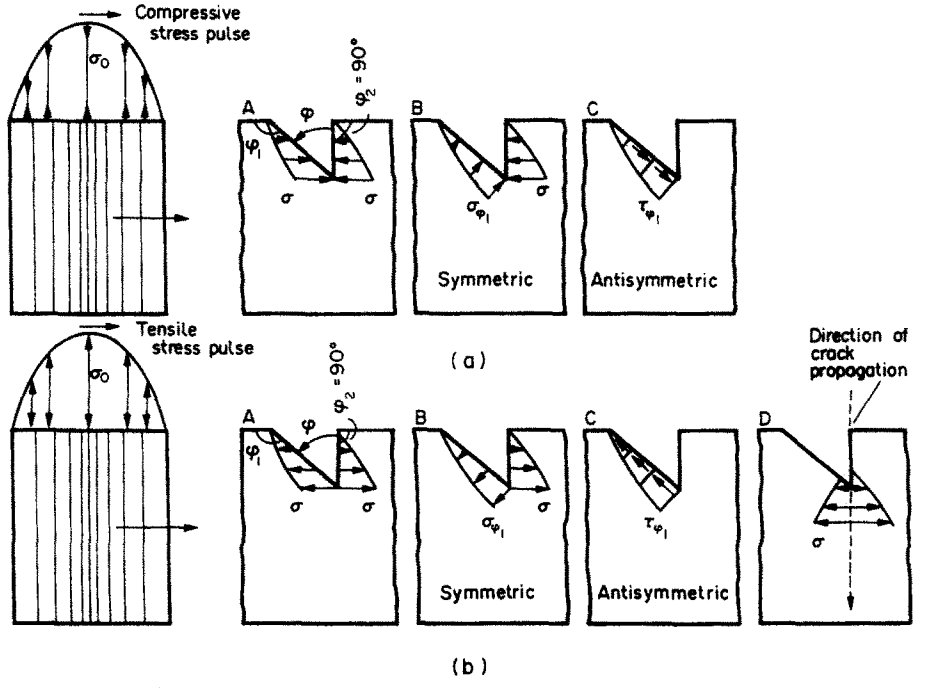


Fig. 4. Diffraction of a stress pulse at an oblique V-notch of initial length depth $a_0$: (a) compressive stress pulse; (b) tensile stress pulse, $\varphi_1 > 90°$ and $\varphi_2 = 90°$.

(Fig. 3(b) C). Thus, the apex of the notch is under the influence of a tensile stress field, $\sigma$, which is propagating radially in front of the apex of the notch. This tensile stress field presents a singularity depending on the angle $\varphi$, and causes the incubation and eventual initiation of propagation of a crack along a direction normal to the direction of propagation of the stress pulse.

Figure 4 presents the same phenomena as in Fig. 3, but for the case when the V-notch is oblique and the flanks of which subtend the angles $\varphi_1 > \pi/2$ and $\varphi_2 = \pi/2$ with the

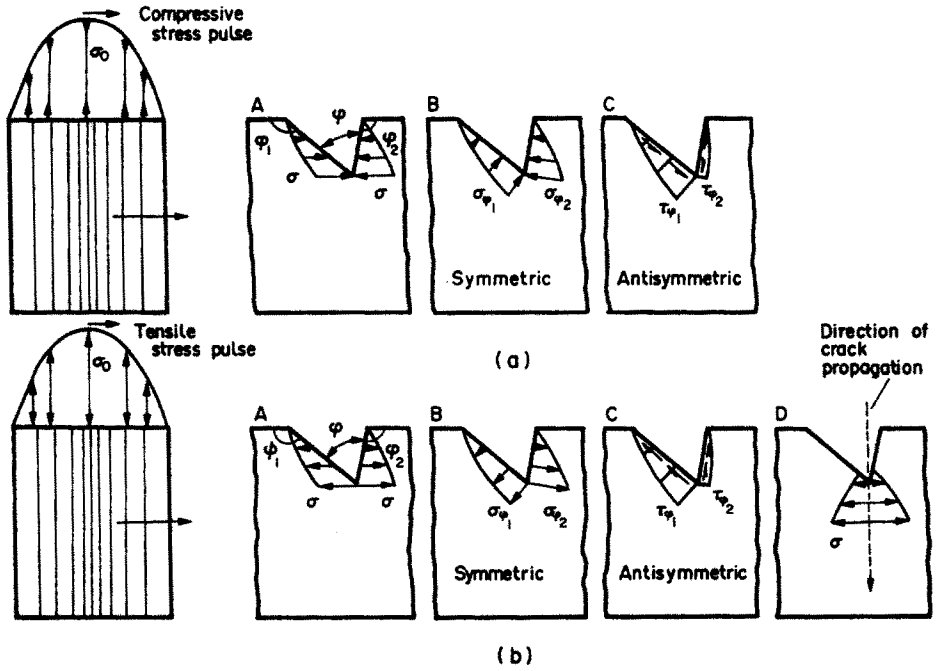


Fig. 5. Diffraction of a stress pulse at an oblique V-notch of initial length depth $a_0$: (a) compressive stress pulse; (b) tensile stress pulse, $\varphi_1 > \varphi_2 > 90°$.

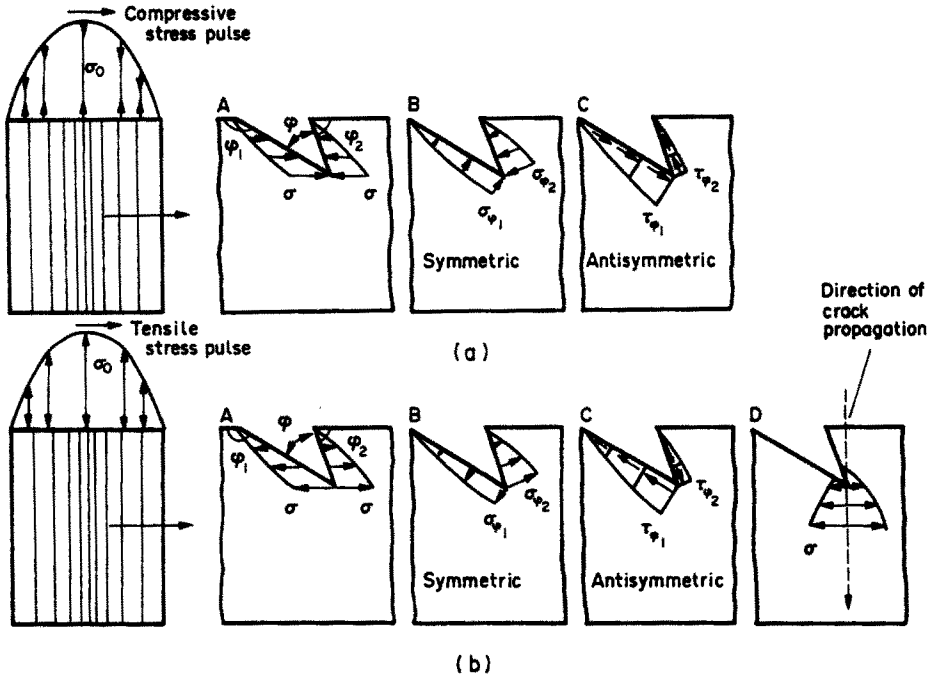


Fig. 6. Diffraction of a stress pulse at an oblique V-notch of initial length depth $a_0$: (a) compressive stress pulse; (b) tensile stress pulse, $\varphi_1 > 90°$, $\varphi_2 < 90°$.

longitudinal boundary of the strip. Now, the compressive stress field introduces normal $\sigma_{\varphi_1}$- and $\sigma_{\varphi_2}$-stresses along the notch flanks (Fig. 4(a) B) and a shear $\tau_{\varphi_1}$-stress (Fig. 4(a) C), whereas, the tensile stress field introduces normal and shear stresses and thus the apex of the notch is under the influence of a tensile stress field, $\sigma$, which causes the eventual initiation of a crack and its propagation. The stress field $\sigma$ varies between 0 and $\sigma_0$. If $\sigma_0 \geqslant \sigma_{cr}$, where $\sigma_{cr}$ is the critical value of stress for the propagation of the crack, phenomena of incubation and propagation will take place, while if $\sigma_0 < \sigma_{cr}$, such phenomena will not take place. So, the propagation phenomena are dependent on the amplitude of the initial stress pulse.

Figure 5 presents the same phenomena as Figs 3 and 4, but, for an oblique V-notch of angles $\varphi_1 > \varphi_2 > \pi/2$. Similarly, Fig. 6 concerns the case of an oblique V-notch of angles $\varphi_1 > \pi/2$ and $\varphi_2 < \pi/2$. In these cases the arrangements of the stress fields are different.

It is worthwhile noticing that the $u$- and $v$-displacements around the apex of the notch have different values and they depend on the values of stresses there. However, the stress intensities at the apex of the notch, as well as on the tips of the propagating cracks may be conveniently and accurately determined by the methods of caustics[23] and pseudo-caustics[24]. On the other hand, the stress fields, which were presented in Figs 3–6, are additionally influenced by the stress waves of the secondary reflections on the free boundaries of the plate. But, the amplitudes of these stress waves are much less than the amplitude of the first, impinging on the notch, stress pulse and so it is assumed that the instantaneous stress fields at the apex and the crack tip will not change significantly by these secondary pulses.

## 4. THE EXPERIMENTAL ARRANGEMENT FOR THE IMPACT TESTS

The experimental set-up of transmitted caustics[21–23, 25] was used in combination with a Cranz–Schardin high-speed camera. The specimens were subjected to a plane compressive stress pulse created by a projectile shot by an air-gun, which was under an air pressure varying between 1.0 and 2.5 bar. The magnitude of the plane stress pulse was about $\varepsilon_{max} = 2.5 \times 10^3$ $\mu$strain[16]. The magnitude of the reflected pulse from the opposite transverse free boundary of the specimen was equal to $2.5 \times 10^3$ $\mu$strain, while the magnitudes of reflected pulses from the notch flanks depended on the angles of incidence[1].

For the experimental study of impact phenomena, notched PMMA plates were used. The dimensions of the specimens were equal to: length $l = 0.300$ m, width $w = 0.040$ m and thickness $d = 0.003$ m (Fig. 1). The angles of the notches $\varphi$ varied between 25° and 120°, while the angles $\varphi_1$ and $\varphi_2$ varied between 30° and 175°. The specimens were suspended in a horizontal position by means of thin and flexible filaments, thus forming a modified Hopkinson bar, and were impacted at their transverse firing ends by a steel sphere impinging on a special flat-pulse forming device. Moreover, the firing ends of the strips were sufficiently far away from the region of the notch, so as to assure plane stress waves arriving at this zone. The dynamic properties of PMMA were calculated for the appropriate pulse velocities in simple bar tests[26] and found to be: modulus of elasticity $E = 4.3 \times 10^9$ N m$^{-2}$, Poisson's ratio $\nu = 0.34$ and the stress optical constant for transmitted light rays $c_t = -0.74 \times 10^{-10}$ m$^2$ N$^{-1}$.

According to the method of transmitted caustics, a divergent light beam impinges on the specimen in close vicinity of the bottom of the notch and the transmitted rays are received on a reference plane, parallel to the plane of the specimen. These rays are deviated in different directions according to the law of refraction and they are concentrated along a strongly illuminated curve, which is called the caustic. From the size and the angular displacement, $\omega$, of the axis of symmetry of the caustic, relative to the crack, or notch axis, it is possible to calculate the stress intensity factors $K_I$ and $K_{II}$, provided that the order of singularity at the tip or the apex of the discontinuity is known[21].

The complex stress intensity factor $K$ for the case of a sharp V-notch is given by[21, 22]

$$|K| = \delta_\lambda(\varphi)\,(D_t/\lambda_m)^{(2-\lambda)}/|C| \tag{1}$$

where $\delta_\lambda(\varphi)$ is a correction factor, $\lambda$ is the order of singularity which depends on the angle of the notch, $\varphi$, $D_t$ is the maximum transverse diameter of the caustic, which is formed around the apex of the notch, $\lambda_m$ is the magnification ratio of the optical set-up and $C$ is an overall constant, which is given by

$$C = \frac{z_0 d c_t}{\lambda_m (2\pi)^{1/2}} \tag{2}$$

where $z_0$ is the distance between the specimen and the reference plane, $d$ is the thickness of

Table 1. Typical values for the order of singularity, $\lambda$, and the correction factor, $\delta_\lambda(\varphi)$, for sharp V-notches the flanks of which are subtending an angle $\varphi$[22]

| $\varphi$ (deg.) | $\lambda$ | $\delta_\lambda(\varphi)$ |
|---|---|---|
| 0 | −0.50000 | 0.0745 |
| 30 | −0.49855 | 0.0748 |
| 60 | −0.48778 | 0.0771 |
| 90 | −0.45552 | 0.0846 |
| 120 | −0.38427 | 0.1064 |
| 150 | −0.24802 | 0.1874 |
| 180 | −0.00000 | ∞ |

the specimen and $c_t$ is the optical constant of the material for transmitted light rays. In the optical set-up used in the tests $z_0$ and $\lambda_m$ had the values $z_0 = 0.80$ m and $\lambda_m = 0.75$. The stress intensity factors $K_I$ and $K_{II}$ are given by

$$K_I = \frac{|K|}{(1+\mu^2)^{1/2}} \tag{3}$$

$$K_{II} = \mu K_I = \frac{\mu|K|}{(1+\mu^2)^{1/2}} \tag{4}$$

with

$$\mu = \tan(\lambda\omega) \tag{5}$$

where $\omega$ is the angular displacement of the axis of the caustic relative to the axis of symmetry of the crack or notch. The quantities $\lambda$ and $\delta_\lambda(\varphi)$ are taken from Table 1, given in Ref. [22].

When a crack nucleates at the apex of the notch the order of singularity $\lambda$, which is different from $\lambda = -0.5$ changes abruptly to $-0.5$, which corresponds to the singularities of crack tips. Then, the stress intensity factors $K_I$ and $K_{II}$ are calculated according to the theory of dynamic caustics at the propagating crack tips[18, 25]. The respective relations valid for the calculation of the $K_I$- and $K_{II}$-SIFs are

$$K_I = \frac{2(2\pi)^{1/2}}{3z_0 d\lambda_m^{3/2} c_t}\left(\frac{D_{t,l}^{max}}{\delta_{t,l}^{max}}\right)^{5/2} \tag{6}$$

$$K_{II} = K_I \tan\left(\frac{\omega}{2}\right) \tag{7}$$

where $D_{t,l}^{max}$ expresses the maximum, either transverse (t), or longitudinal (l), diameters of the caustic and $\delta_{t,l}^{max}$ are the respective correction factors for these diameters, which are dependent on the crack velocities and are given by nomograms in Refs [18, 25].

## 5. EXPERIMENTAL RESULTS AND DISCUSSION

In order to exemplify the sequence of phenomena described in the previous sections and concerning the reinforcement or weakening of the propagating stress pulses in an obliquely notched strip, due to successive reflections along the boundaries of the strip and the flanks of the notch, as well as due to diffraction of stress waves at the apex of the notch, a series of tests were undertaken, where the loading and unloading of the notch was recorded by applying the method of caustics.

Figure 7 presents a series of photographs for a PMMA strip, containing a symmetric V-notch of initial length $a_0 = 0.010$ m. The angles of the notch were $\varphi = 120°$, $\varphi_1 = \varphi_2 = 150°$. The air pressure in the gun in this case was equal to 1.0 bar. Figure 8 presents a series of photographs for a PMMA strip, containing a symmetric V-notch of initial length $a_0 = 0.009$ m. The angles of the notch were in this case $\varphi = 160°$, $\varphi_1 = \varphi_2 = 170°$. Moreover, the air pressure in the gun in this case was equal to 2.5 bar.

The series of photographs in Figs 7 and 8 indicate the influence of the arriving tensile stress pulses at the apices of the V-notches. Indeed, at these instants caustics are formed of the type of tensile caustics (almost circular), which are continuously increasing in size, since the intensity of the stress pulse is increasing with time. Then, the values of the respective SIFs at the apices of the notches, $K_I$, are increasing up to a certain critical value, for initiating a crack propagation at the bottoms of the notches (Figs 7(6) and 8(17)).

Subsequently, the cracks are propagating with continuously increasing velocities, radiating also from their tips stress waves (Figs 7(7, 9, 10) and 8(18, 10)). These stress waves are of the Rayleigh type as it has been shown in Ref. [27]. When the cracks approach the opposite longitudinal boundaries of the strips, their velocities are progressively and rapidly reduced and the respective values of SIF are also reduced, as it may be evaluated from the progressive reduction of the sizes of the caustics at these neighbourhoods (Fig. 7(14)). These reductions of $v_c$ and $K_I^{dyn}$ are due to the interferences of the progressing crack tips and the stress waves already reflected from the opposite boundaries of the strips.

Another important phenomenon detected only in the photographs of Fig. 8 is the phenomenon of reflection of the Rayleigh waves at the opposite longitudinal boundaries of the strips as soon as the crack tips attain them and the strips are separated into two pieces. In these instants reflected Rayleigh waves radiate from the new source of reflected energy, that is the point of intersection of the crack and the opposite longitudinal boundary.

On the other hand, after the passing over of the extensional stress pulses and the annulling of the crack velocities $v_c$ and of the $K_I$-SIFs, the extensional stress pulses are reflected from the free transverse ends of the strips and return as compressive pulses. When these pulses pass through the flanks of the cracks the two separated parts of the strips collide with each other thus creating strong deformations along the whole lips of the cracks. Thus, Figs 7(16–19) and 8(20–24) present a series of connected black dots, which are secondary caustics created from the partial contacts of the two lips of the cracks. The variations of their sizes and forms during the evolution of the phenomena indicate the variability of these dynamic after effects until their total attenuation.

Of importance are two phenomena indicated in Figs 8(20) and (23). In Fig. 8(20) together with the Rayleigh waves radiating from the extremity of the crack there is also a black dot of significant size travelling with the same velocity as the Rayleigh waves and which represents the amount of energy reflected from the opposite boundary and travelling back inside the plate.

It has been shown previously that it is possible, by defining the shapes of these caustics and measuring their characteristic dimensions, to evaluate the forces applying at the boundaries creating these caustics[28–30]. Since the area enclosed by the caustic corresponds to the elastic energy transmitted to the plate by the external loading[31], it is possible to evaluate readily the amount of energy reflected backwards from the opposite boundaries of the already broken strips. A complete analysis of this inverse problem is in progress[32].

A similar phenomenon but of a different nature is presented in Fig. 8(23). Here the two lips of the cracks that broke the specimens are in partial contact due to the zig-zagging of initial paths. Thus, the compressive stress pulses partially close these lips and create areas of contact with strong caustics and their extremities and pseudocaustics along the rest of their contact zones. Of importance are also the traces of a dilatational wave represented by a dim white arc and a shear wave following the first, represented by a black intense arc of smaller radius than the previous one[32].

The same phenomena of contact during the passage of the compressive stress pulse appear in Figs 7(16, 18, 19), but here the contact of the opposite lips is rather smooth and the caustics appear as small beads following each other in close proximity.

The differences in the behaviour of the two strips in Figs 7 and 8 are due to the fact

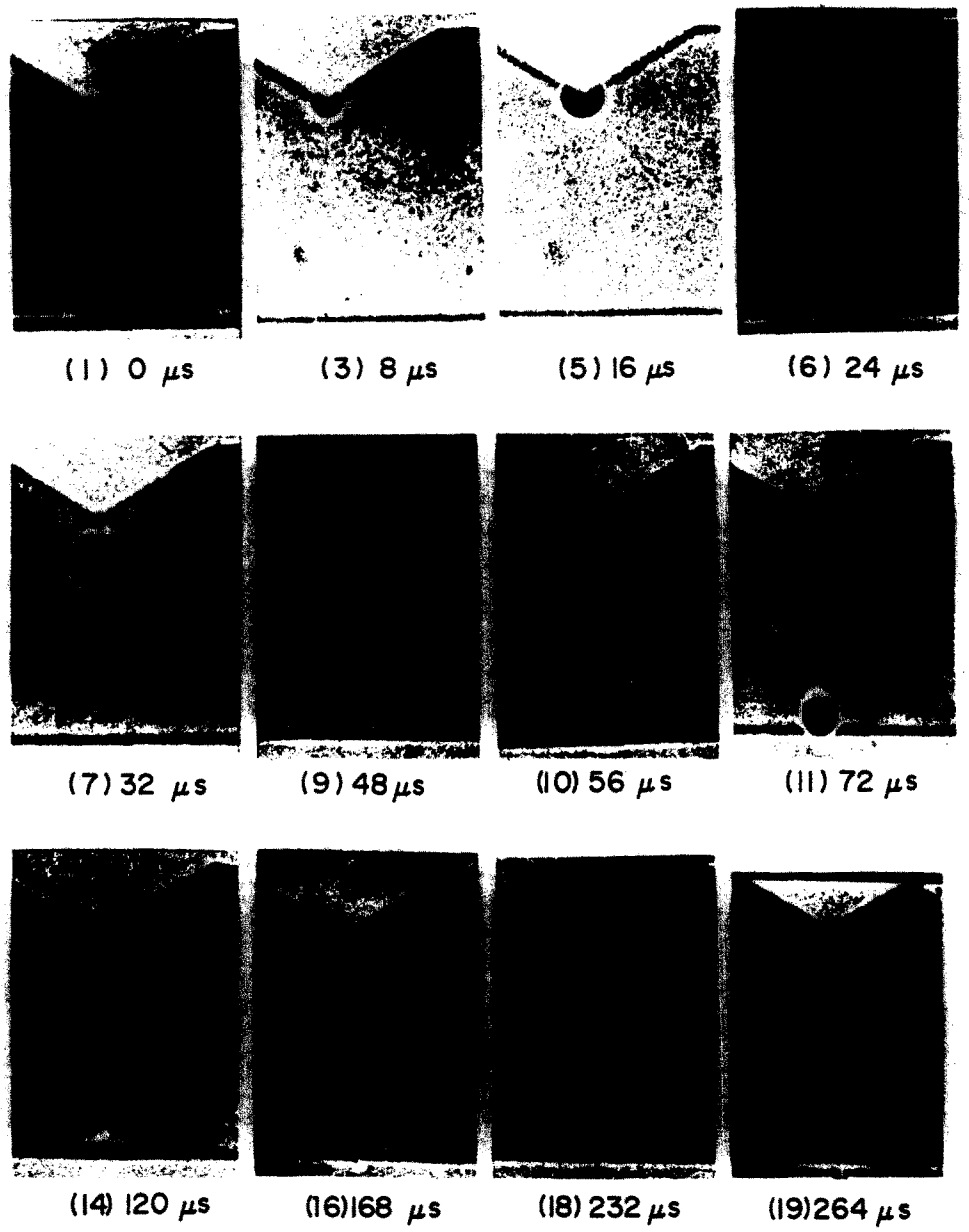


Fig. 7. Series of photographs obtained with a high-speed camera in a V-notched PMMA strip with $a_0 = 0.010$ m, $\varphi = 120°$ and $\varphi_1 = \varphi_2 = 150°$. The projectile shot by the air-gun was under an air pressure of 1.0 bar.

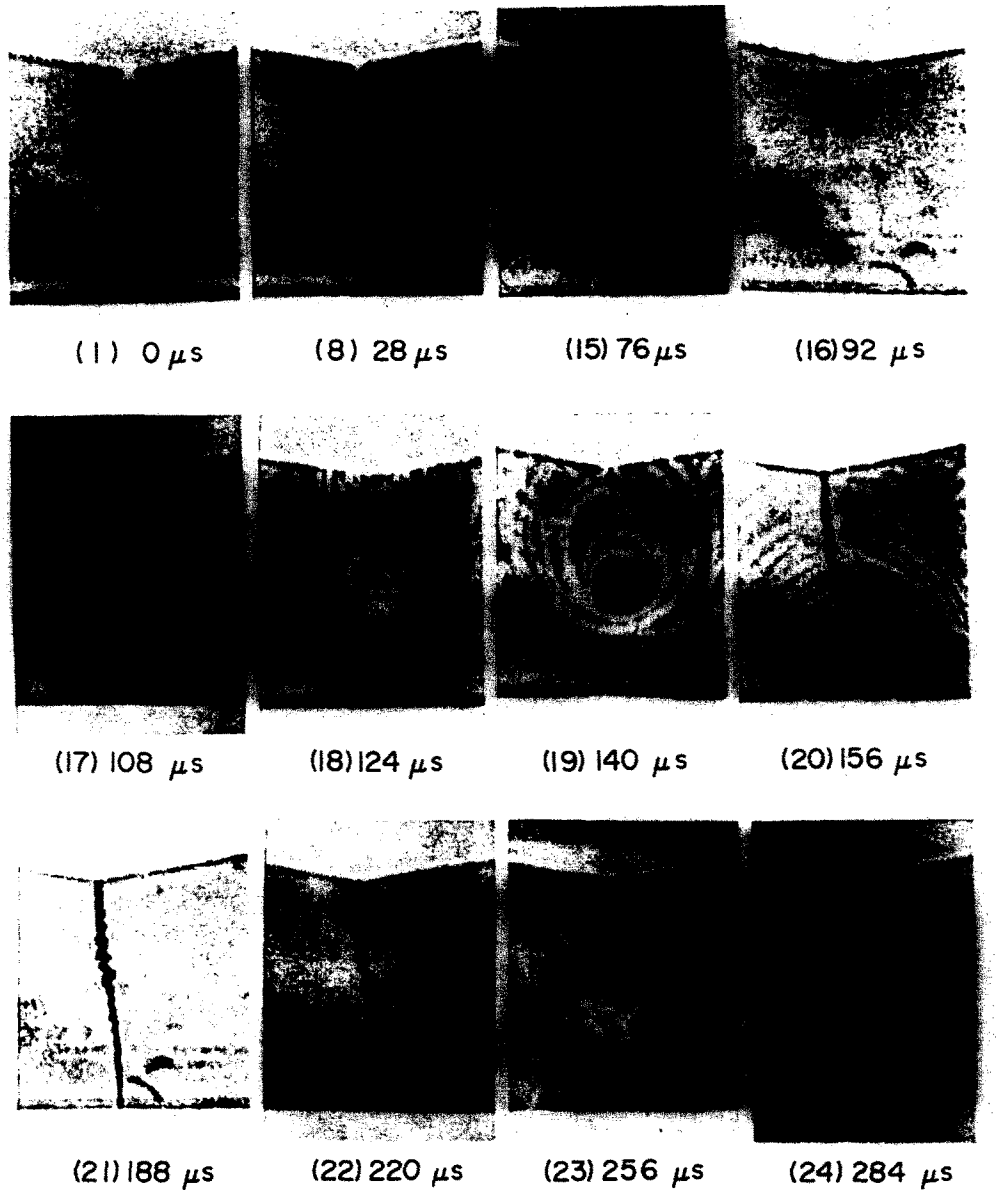


Fig. 8. Series of photographs obtained with high-speed camera in a V-notched PMMA strip with $a_0 = 0.009$ m, $\varphi = 160°$ and $\varphi_1 = \varphi_2 = 170°$. The projectile shot by the air-gun was under an air pressure of 2.5 bar.

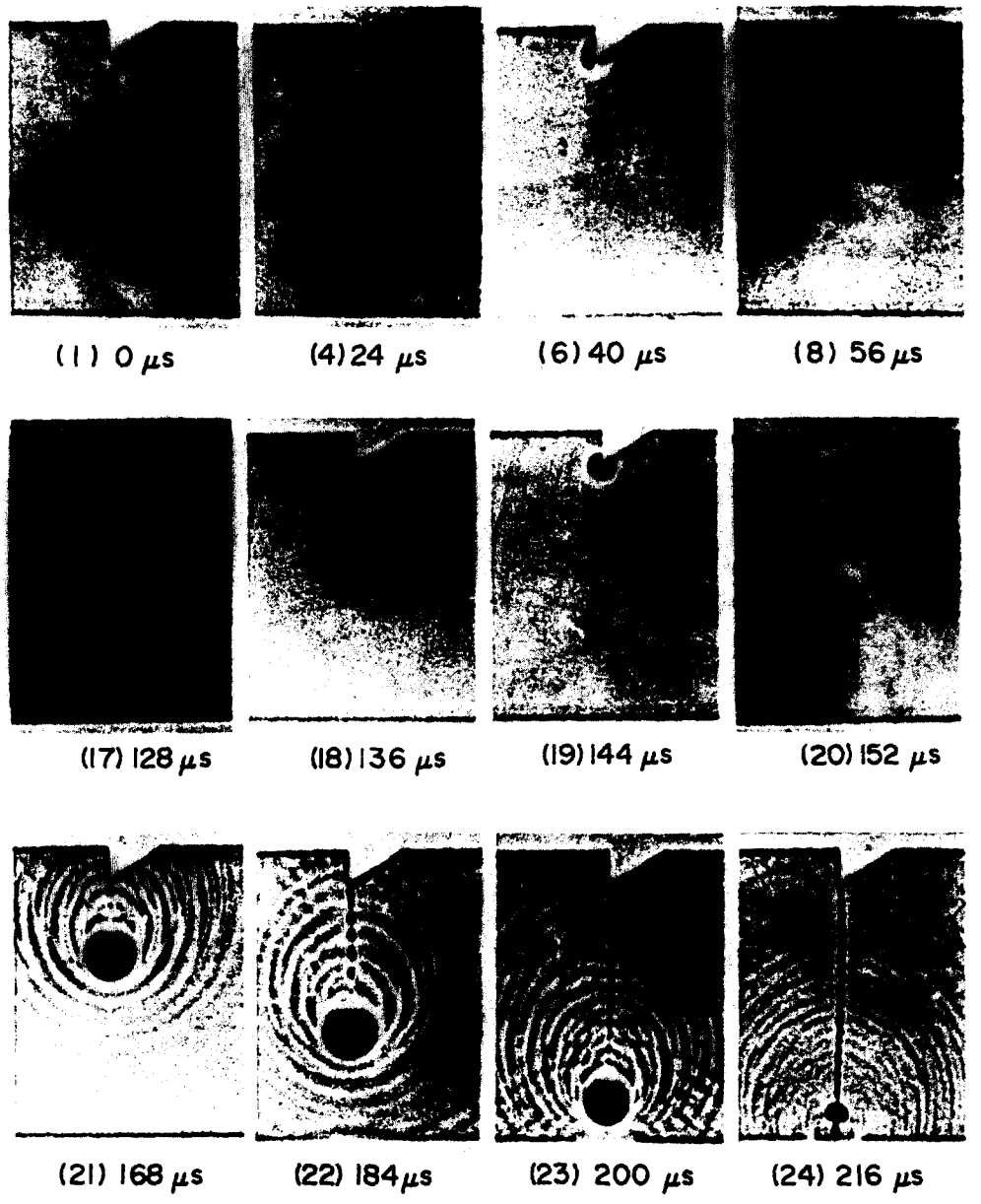


Fig. 10. Series of photographs obtained with a high-speed camera in a V-notched PMMA strip with $a_0 = 0.005$ m, $\varphi = 60°$ and $\varphi_1 = 90°$, $\varphi_2 = 150°$. The projectile shot by the air-gun was under an air pressure of 1.3 bar.

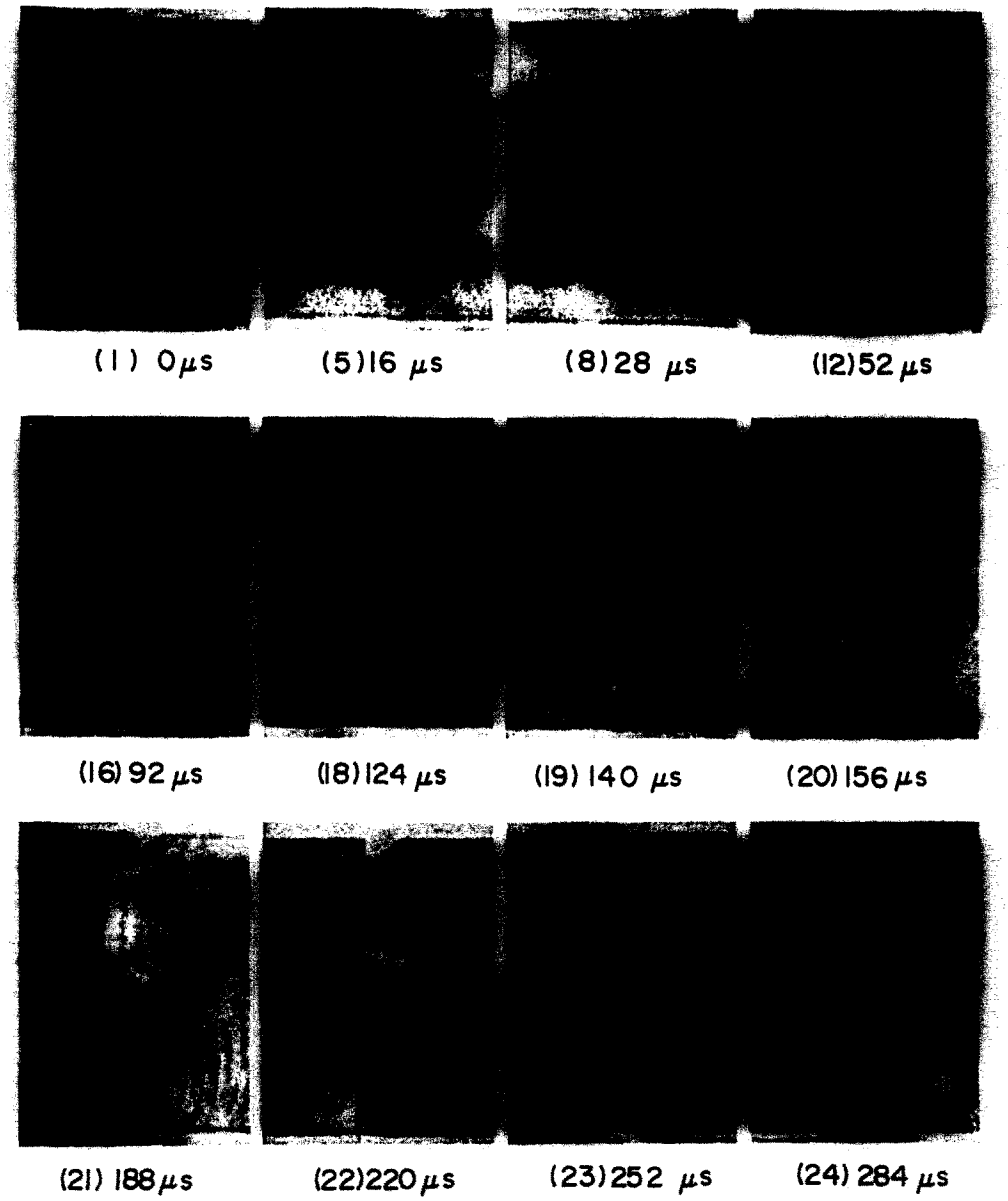


Fig. 12. Series of photographs obtained with a high-speed camera in a V-notched PMMA strip with $a_0 = 0.004$ m, $\varphi = 50°$ and $\varphi_1 = 85°$, $\varphi_2 = 140°$. (Air pressure $p = 1.3$ bar.)

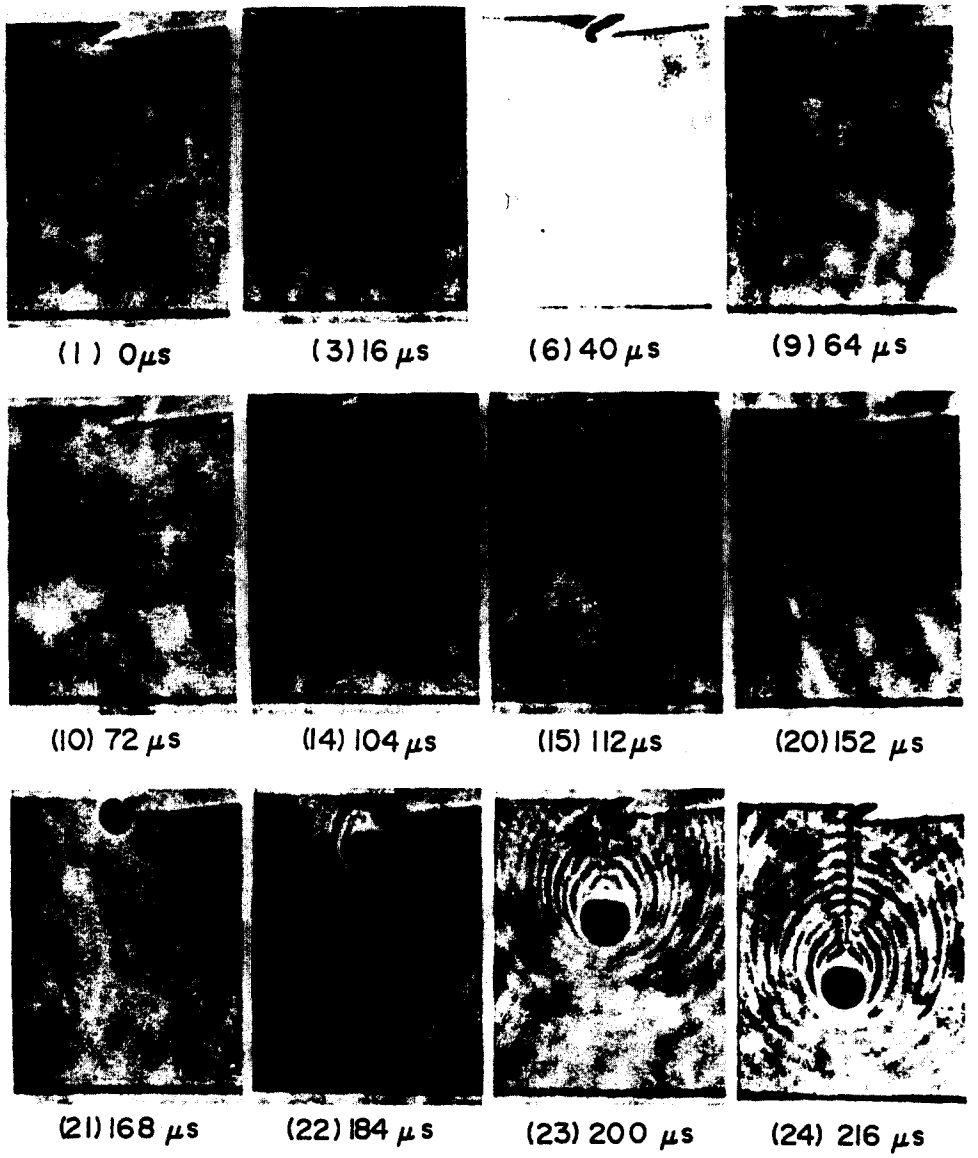


Fig. 14. Series of photographs obtained with a high-speed camera in a V-notched PMMA strip with $a_0 = 0.0025$ m, $\varphi = 25°$ and $\varphi_1 = 30°$, $\varphi_2 = 175°$. (Air pressure $p = 1.3$ bar.)

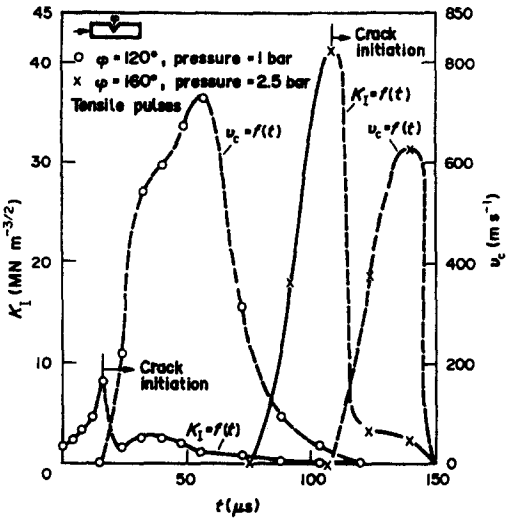


Fig. 9. Variation of the stress intensity factor, $K_I$, and the crack velocity, $v_c$, vs time for the experiments of Figs 7 and 8.

that the angles $\varphi$ for the two cases are $\varphi = 120°$ and 160°, respectively. Because of this difference between the angles $\varphi$ of the notches, the stress pulse in the second case must be much stronger than in the first case, in order to create fracture with such an obtuse notch. Indeed, the stress pulse in the second case is 2.5 times larger than the first one. This explains the stronger deformation phenomena appearing in the strip after its total failure and the large deformations of the flanks of the notch as well as the separated lips of the already broken crack.

Figure 9 presents the variations of the crack velocities, $v_c$, and the respective stress intensity factors, $K_I$, vs real time from the instant of the arrival of the pulses at the neighbourhood of the notches for the two cases studied in Figs 7 and 8, respectively. It may be first remarked that the loading phenomena of the notches and the crack propagations appear earlier for the sharper notch with $\varphi = 120°$ and afterwards for the obtuser notch with $\varphi = 160°$. In both cases there is an abrupt increase of the stress intensity factor values up to a maximum when cracks initiate at the bottom of the notches and then an initial abrupt decrease of $K_I$ followed by a smoother and wavy attenuation of $K_I$ presenting a rather shallow secondary maximum. The crack velocities in both cases follow similar bell-shaped curves with smoother slopes for the increasing branches and abrupt, afterwards smoothly attenuating, decreasing branches.

The differences in total times for the propagations of the cracks are due to the differences in the intensities of the stress pulses. Indeed for the 120°-notch the total time of crack propagation is $t_{120} = 107$ μs, whereas for the 160°-notch this time is only $t_{160} = 41$ μs. The ratio $t_{120}/t_{160}$ is approximately equal to 2.5, that is the inverse ratio of the applied stress pulses to the strips.

From Fig. 9 it may be remarked that, while for the sharper notch, fracture is achieved under small applied pressure and low values of $K_I$, for the obtuser notch high applied pressures are necessary to initiate fracture which starts at high values of $K_I$. On the contrary the average crack velocities are high for the 120°-notch and low for the 160°-notch.

Finally, since the initial notches are symmetric to the transverse direction of the strip and to the front of the applied plane stress pulses only the $K_I$-SIF is operative and $K_{II} = 0$ everywhere.

Another interesting remark is that while before the initiation of propagation of the cracks the values for $K_I$ are in general high, after initiation of propagation of the cracks they are reduced abruptly and considerably to much lower values. This phenomenon may be explained by the fact that the orders of singularities at the bottoms of the notches are much lower than the order of singularity at a crack tip ($\lambda = -1/2$). Thus for $\varphi = 120°$ it may be found from Ref. [22] that $\lambda_{120°} = -0.38427$ and for $\varphi = 160°$ that $\lambda_{160°} = -0.16530$.

The transition of the order of singularity from its value corresponding to the respective notch to the order $\lambda = -1/2$ for a crack tip is made by consuming some internal energy which reduces the caustics at this transition period and the values of $K_I$ considerably.

Figure 10 presents a series of photographs depicting the mode of loading and fracture of a thin strip made of PMMA and containing a V-notch of initial length $a_0 = 0.005$ m and angles $\varphi = 60°$, $\varphi_1 = 90°$ and $\varphi_2 = 150°$. The applied pressure by the air-gun in the series of tests with strips of such notches was 1.3 bar.

Figure 11 presents the variation of the crack velocity, $v_c$, and the components of the stress intensity factor vs time for the test presented in Fig. 10.

The photographs of Fig. 10 indicate that the orthogonal notch, loaded from the side of its normal flank, is strained according to the model of Fig. 4. The compressive pulse (Figs 10(1–17)) loads the V-notch with a compression stress and a shear stress component of high value. In this way a caustic is formed along the normal flank of the notch of the compression type. This caustic also presents an angular displacement due to the shear stress, which contributes to the creation of the $K_{II}$-SIF. Relations (3) and (4) allow the evaluation of the $K_I$- and $K_{II}$-SIFs from its transverse diameter and its angular displacement.

Subsequently the stress pulse, after a reflection along the opposite transverse boundary of the strip returns to the notch zone as a tensile pulse and loads accordingly the V-notch. Caustics are formed of the tensile type (almost circular), corresponding to Figs 10(18–20). This loading of the bottom of the notch results in a nucleation and propagation of a crack indicated in Figs 10(20–23). During the crack propagation, emission of Rayleigh stress waves accompanies the propagation of the crack (Figs 10(21–23)), whereas after the exit of the crack from the opposite longitudinal boundary and the total separation of the strip into two pieces a backwards travelling caustic in Fig. 10(24) indicates a backwards reflected energy quantity which is proportional to the size of the caustic which travels with the Rayleigh velocity and does not attenuate during propagation.

The sizes and orientations of the caustics as well as their exact positions suffice to evaluate the crack-tip velocities and the instantaneous values of the dynamic $K_I$- and $K_{II}$-stress intensity factors.

Figure 11 presents the variation of the crack-tip velocities and the values of the $K_I$- and $K_{II}$-dynamic SIFs, vs time. It is clear from these plots that again $K_I$ and $K_{II}$ attain large values during the passage of the compressive pulse which were afterwards reduced considerably in the period of the passage of the tensile stress pulse, whereas the values of the crack propagation velocity remain rather high.

It is worthwhile remarking an interesting phenomenon appearing in Figs 10(21–24) of the secondary caustics formed at the intersections of the crack path, behind the crack tip, and the traces of the Rayleigh waves. These caustics indicate the amount of deformation at the Rayleigh fronts and they may yield the means of evaluating the energies carried with them. A calculation of these quantities is undertaken in Ref. [32]. Similar and very pronounced caustics formed at the intersections of the Rayleigh fronts and the paths of the cracks were already indicated in Ref. [33] and their importance was stated there.

Finally in Figs 12 and 14 V-notches of the form of saw-teeth cut-out in PMMA strips were studied under the influence of initial compressive pulses created by air-gun pressures equal to 1.3 bar. In Fig. 12 the notch had an initial length $a_0 = 0.004$ m and angles $\varphi = 50°$, $\varphi_1 = 85°$ and $\varphi_2 = 140°$, whereas in Fig. 14 the respective values were $a_0 = 0.0025$ m, $\varphi = 25°$, $\varphi_1 = 30°$ and $\varphi_2 = 175°$.

These two cases are of interest to show the phenomenon of caging in of the stress pulses inside the protrusions formed by the longitudinal boundaries of the strips and the less oblique flanks of the V-notches. As it is shown in the photographs of Figs 12 and 14 the loading modes of the V-notches follow the patterns of stress distributions shown in Fig. 6 by applying first the compressive pulses to the notches and afterwards the tensile stress pulses, thus creating stress distributions along the flanks of the notches described by this model. During the period of the influence of the compressive pulse a strong shear loading along the flanks of the notches is apparent (see Figs 12(1–16) and 14(3–15)). Another important remark is that during the caging-in phenomena not only the flanks of the notches are highly loaded, but also the parts of the longitudinal boundaries lying on the sides of

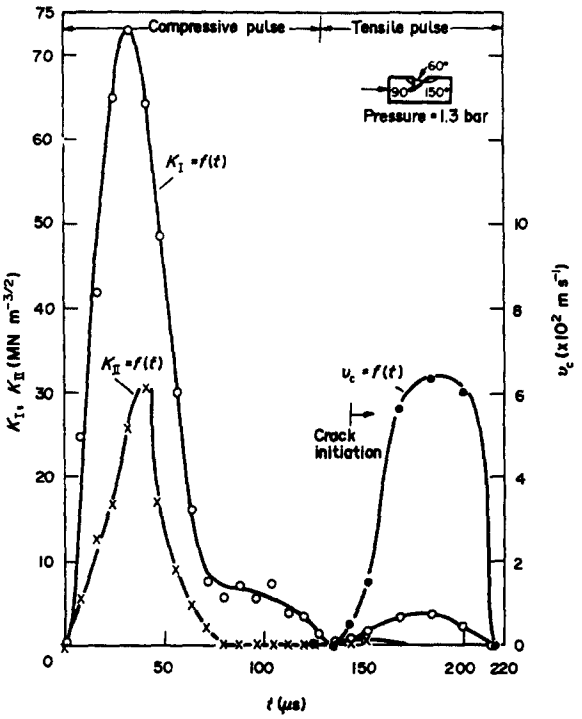


Fig. 11. Variation of the stress intensity factors $K_I$ and $K_{II}$ and the crack velocities, $v_c$, vs time for the experiment of Fig. 10.

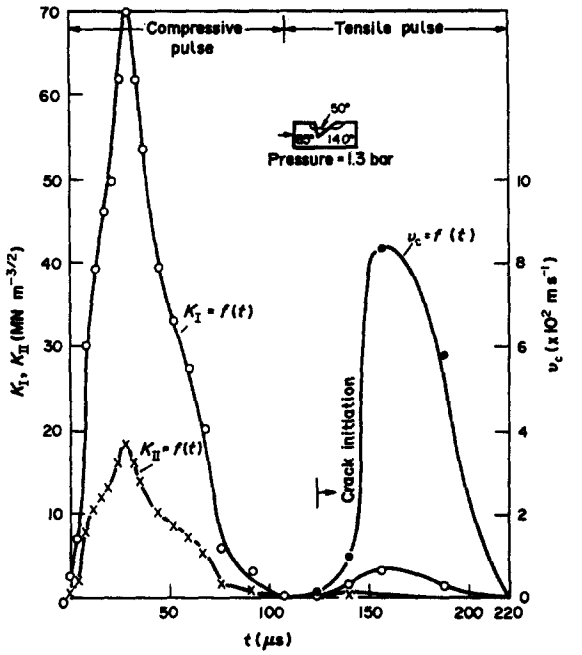


Fig. 13. Variation of the stress intensity factors $K_I$ and $K_{II}$ and the crack velocities, $v_c$, vs time for the experiment of Fig. 12.

the coming pulses, so that intense pseudocaustics appear along these boundaries in Figs 12(5–12) and 14(3–9), the higher loadings of these boundaries being shown in Figs 12(8) and 14(6).

Again during the compressive pulse loadings of the notches the values of $K_I$ and $K_{II}$ increase rapidly and attain high values as it is shown in Figs 13 and 15, respectively, where the variations of $v_c$ and of $K_I$- and $K_{II}$-SIFs are plotted vs time.

During the phase of loading of the notches with the reflected tensile pulses cracks are initiated at the bottom of the notches, which are propagated straight ahead under lower

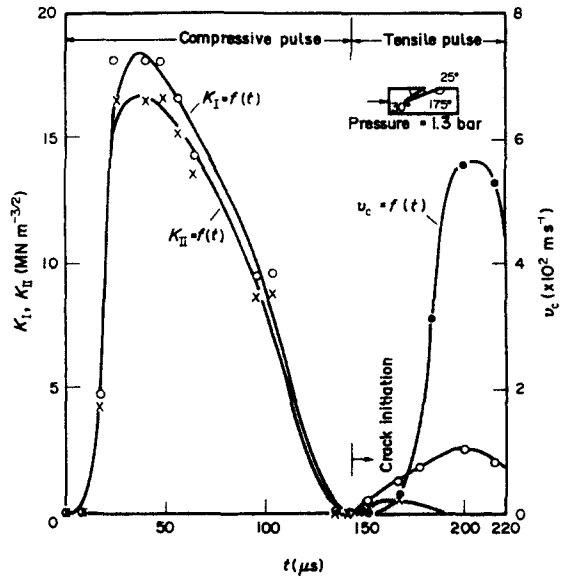


Fig. 15. Variation of the stress intensity factors $K_I$ and $K_{II}$ and the crack velocities, $v_c$, vs time for the experiment of Fig. 14.

values of the $K_I$-stress intensity factor for reasons explained already in the first series of tests. The propagating cracks were accompanied along the whole widths of the strips by Rayleigh waves and they were also reflections of some parts of the energies stored at the cracks which travelled backwards with the Rayleigh wave velocities for PMMA.

An important remark with the test of Fig. 12 is that, at the relaxing of the strip after complete fracture (Fig. 12(23)), the returning backwards reflected compressive stress pulse is compressing the totality of the flanks of the broken specimen, creating significant sizes of caustics at points of load concentrations whereas simultaneously loading both flanks of the notch.

This phenomenon of compressive loading of the flanks of cracks and faults, which is well described in geomechanics especially in cases of seismic phenomena, is several times in our experiments satisfactorily recorded in the laboratory for the first time. In the tests of Fig. 14 the recording was concentrated in the early phases of the caging-in phenomenon in the acute wedge between the longitudinal boundary and the flank of the notch, which is totally under intense deformation presenting a combined mode II and III caustic in Fig. 14(14) which is transformed in Fig. 14(15) into a higher order caustic with an oblique cross shape and is incapable of being described by the existing theory of caustics, since being a "higher order catastrophe" necessitating a different mathematical treatment.

Finally, it is worthwhile pointing out that in all cases of asymmetric notches the propagating cracks were mainly under mode I deformations and the values of the $K_{II}$-components of SIF took only insignificant values and only for the early stages of crack propagation.

## 6. CONCLUSIONS

The experimental study of the impact phenomena in strips containing sharp V-notches along one of their longitudinal boundaries, based on the method of caustics, revealed important features of the dynamic behaviour of structures.

Thus, reflections of the initial compressive stress pulses along all the boundaries, longitudinal, transverse, and notch flanks, gave secondary tensile stress pulses and created longitudinal and transverse stress waves, which diffracted from the bottom of the notches and interfered between them creating complicated states of loading of the plates.

Depending on the obliqueness of the notch flanks and especially the front flank receiving first the influence of the coming stress pulse, caging-in phenomena appeared in

the protrusions between the notches and the boundaries, which multiplied the phenomena of reflections and sometimes resulted in fracture of these protrusions.

The compressive stress pulses always loaded the flanks of the notches and created stress intensities at their apices of high values and both components of SIFs.

The tensile stress pulses always resulted in nucleating cracks emanating from the bottom of the notches, which propagated straight ahead along transverse directions under mode I conditions and fractured the strips. The values of $K_I$- and $K_{II}$-SIFs during the nucleation and propagation of the cracks were abruptly reduced from their high values during the influence of the compressive pulses. The $K_I$-SIF varied smoothly, presenting some flat maxima, whereas the $K_{II}$-SIF was rapidly attenuated.

The propagation of the cracks was followed by Rayleigh waves creating distinct traces and developing secondary caustics at their intersections with the lips of the cracks. From these caustics it is possible by an inverse method of caustics to evaluate the elastic energy carried forward by each Rayleigh wave.

Phenomena of reflection of waves from the opposite longitudinal boundaries of the strips are detected and similarly the travelling backwards waves and their caustics along the crack lips give a means of evaluating the reflected elastic energy from the boundaries of the strips.

Finally, an important phenomenon well known in geomechanics, that is of the closure of the separated lips of cracks or faults by travelling backwards compressive stress pulses was readily detected and an analysis of the caustics formed by the partial contacts of opposite lips of the cracks may give a powerful means of studying such phenomena.

## REFERENCES


1. H. Kolsky, *Stress Waves in Solids*. Dover, New York (1963).
2. J. W. C. Sherwood, Elastic wave propagation in a semi-infinite solid medium. *Proc. Phys. Soc.* **71**, 207 (1958).
3. L. Cagniard, *Reflection and Refraction of Progressive Seismic waves*. McGraw-Hill, New York (1962).
4. W. M. Ewing, W. S. Jardetsky and F. Press, *Elastic Waves in Layered Media*. McGraw-Hill, New York (1957).
5. Miklowitz, Elastic waves created during tensile fracture. *J. Appl. Mech.* **20**, 122 (1952).
6. V. R. Thiruvenkatachar, *Stress Waves Propagation in Materials. Proc. Int. Symp.* (Edited by N. Davids), p. 1. Interscience, London (1960).
7. R. J. Eichelberger, *Stress Waves Propagation in Materials. Proc. Int. Symp.* (Edited by N. Davids), p. 133. Interscience, London (1960).
8. K. B. Broberg, *Stress Waves Propagation in Materials. Proc. Int. Symp.* (Edited by N. Davids), p. 229. Interscience, London (1960).
9. J. S. Rinehart, *Stress Waves Propagation in Materials. Proc. Int. Symp.* (Edited by N. Davids), p. 247. Interscience, London (1960).
10. L. B. Freund, Crack propagation in an elastic solid subjected to general loading—III. Stress wave loading. *J. Mech. Phys. Solids* **21**, 47 (1973).
11. L. B. Freund, Crack propagation in an elastic solid subjected to general loading—IV. Obliquely incident stress pulse. *J. Mech. Phys. Solids* **22**, 137 (1974).
12. H. Schardin, Velocity effects in fracture. In *Fracture* (Edited by B. L. Averbach, D. K. Felbeck, G. T. Hahn and D. A. Thomas). Wiley, New York (1959).
13. J. F. Kalthoff and D. A. Shockey, Instability of cracks under impulse loads. *J. Appl. Mech.* **48**, 986 (1977).
14. A. S. Kobayashi, S. Mall and A. F. Emery, *Fracture 1977. Advances in Research on the Strength and Fracture of Materials (4th Int. Conf. on Fracture*, 19–24 June 1977, Waterloo, Ont.) (Edited by D. M. R. Taplin), Vol. 3A, p. 79. Pergamon Press, New York (1978).
15. H. H. Homma, T. Ushiro and H. Nakazawa, Dynamic crack growth under stress wave loading. *J. Mech. Phys. Solids* **27**, 151 (1979).
16. P. S. Theocaris and F. Katsamanis, Response of cracks to impact by caustics. *Engng Fract. Mech.* **10**, 197 (1978).
17. P. S. Theocaris and A. Serafetinides, Propagation of a slant crack under impact studied by caustics. *Int. J. Impact Engng* **2**(3), 251 (1984).
18. P. S. Theocaris and G. A. Papadopoulos, Elastodynamic forms of caustics for running cracks under constant velocity. *Engng Fract. Mech.* **13**, 683 (1980).
19. P. S. Theocaris and G. A. Papadopoulos, The dynamic behaviour of an oblique edge-crack under impact loading. *J. Mech. Phys. Solids* **32**, 281 (1984).
20. P. S. Theocaris, Concept of mesophase. Mechanisms of crack propagation. In *Metal-filled Polymers. Properties and Applications* (Edited by S. K. Battacharya), Chap. 5. Dekker, New York (1986).
21. P. S. Theocaris, Stress and displacement singularities near corners. *J. Appl. Math. Phys. (ZAMP)* **26**, 77 (1975).
22. J. N. Prassianakis and P. S. Theocaris, Stress intensity factors at V-notched elastic, symmetrically loaded, plates by the method of caustics. *J. Phys. D: Appl. Phys.* **13**, 1043 (1980).

23. P. S. Theocaris, Elastic stress intensity factors evaluated by caustics. In *Mechanics of Fracture 7* (Edited by G. Sih), Chap. 3. Nijhoff, The Hague (1981).
24. P. S. Theocaris, Experimental study of plane elastic contact problems by the pseudocaustics method. *J. Mech Phys. Solids* **27**(1), 15 (1979).
25. P. S. Theocaris and G. Papadopoulos, Mixed-mode dynamic stress-intensity factors from caustics. *ASTM STP 791* **II**, 320 (1983).
26. F. Katsamanis, D. Raftopoulos and P. S. Theocaris, Static and dynamic stress intensity factors by the method of transmitted caustics. *J. Engng Mater. Technol.* **99**, 105 (1977).
27. P. S. Theocaris and H. G. Georgiadis, Emission of stress waves during fracture. *J. Sound Vibr.* **92**(4), 517 (1984).
28. P. S. Theocaris, Stress singularities at concentrated loads. *Expl. Mech.* **13**(12), 511 (1973). See also: P. S. Theocaris, Stress singularities due to uniformly distributed loads along straight boundaries. *Int. J. Solids Structures* **9**, 655 (1973).
29. P. S. Theocaris and C. Razem, Deformed boundaries determined by the method of caustics. *J. Strain Analysis* **12**, 223 (1977). See also: P. S. Theocaris and C. Razem, Intensity, slope and curvature discontinuities in loading distributions at the contact of two plane bodies. *Int. J. Mech. Sci.* **21**(6), 339 (1979).
30. P. S. Theocaris, C. Stassinakis and A. Mamalis, Roll pressure distribution and coefficient of friction in hot-rolling by caustics. *Int. J. Mech. Sci.* **25**(11), 833 (1983). See also: P. S. Theocaris, A study of the contact zone and friction coefficient in hot-rolling. *Metal. Forming and Impact Mechanics* (Edited by S. R. Reid). W. Johnson's Commemorative Volume, p. 61 (1985).
31. P. S. Theocaris and N. Joacimides, Some properties of generalized epicycloids to fracture mechanics. *Z. Angew. Math. Mech.* **22**(5), 876 (1971).
32. P. S. Theocaris, On the evaluation of the load and energy distribution in travelling reflected Rayleigh waves by the inverse method of caustics, *Engng Fract. Mech.* (1987), submitted for publication.
33. P. S. Theocaris, Studies of dynamic crack propagation with caustics. In *Collection of Papers Devoted to P. Savic on the Occasion of his Seventieth Birthday* (Edited by M. Garasanin), p. 189. Serbian Academy of Sciences and Arts, Beograd (1980).